Nano Energy 75 (2020) 104976

Contents lists available at ScienceDirect

Nano Energy

journal homepage: http://www.elsevier.com/locate/nanoen

Fast lithium ion transport in solid polymer electrolytes from polysulfide-bridged copolymers

Chengguo Sun [a,b], Zhenxing Wang [a,c], Lichang Yin [a], Shengjun Xu [a,c], Zahid Ali Ghazi [a], Ying Shi [a], Baigang An [b,**], Zhenhua Sun [a], Hui-Ming Cheng [d], Feng Li [a,*]

[a] Shenyang National Laboratory for Materials Science, Institute of Metal Research, Chinese Academy of Sciences, Shenyang, 110016, China
[b] School of Chemical Engineering, University of Science and Technology Liaoning, Anshan, 114051, China
[c] School of Materials Science and Engineering, University of Science and Technology of China, Hefei, 230026, China
[d] Tsinghua-Berkeley Shenzhen Institute, Tsinghua University, Shenzhen, 518055, China

ARTICLE INFO

Keywords:
Lithium batteries
Solid polymer electrolytes
Polysulfide-bridged copolymers
Fast ion conductors

ABSTRACT

Solid polymer electrolytes (SPEs) are being intensively pursued as a means to develop safe, stable and long-life Li-ion batteries. However, the low Li^+ conductivity and transference number in SPEs still impede all-solid-state polymer batteries from practical commercialization. Here, lithium polysulfides that cause a shuttle effect problem in Li–S batteries are reduced on a Poly(ethylene oxide) (PEO) chain as an effective way to stimulate Li^+ transport. It is shown that the product of the reduction (main $–S_4Li$) dramatically increases Li^+ transport while forming a strong interaction with the PEO matrix through intermolecular interactions. In contrast to PEO electrolytes, the $–S_4Li$ grafted electrolyte membranes have a lithium transfer number almost 3 times higher, and the $LiFePO_4$|ScPEO|Li cell shows an ultra-long cycle life exceeding 1200 cycles with a capacity decay of 0.024% per cycle at 1 C. The results reveal lithium polysulfides tremendous potential in a solid-state electrolyte system for improving the ion transport and cycling stability.

1. Introduction

Lithium ion batteries (LIBs) are a commonly used rechargeable battery in portable devices because of their advantages of a larger specific capacity, a higher open-circuit voltage, and lower self-discharge than other secondary batteries available [1–4]. With the ever-increasing demand for LIBs with long-term stability, high-energy density and excellent safety, solid-state electrolytes have been pursued as a promising solution to meet these requirements [5,6]. In particular, solid-state electrolytes have the potential to prevent dendrite growth by slowing deformation of the interface between it and the lithium metal electrode and produce a high capacity [7,8]. Various types of solid-state electrolytes that have been developed can be generally classified into two categories: inorganic solid-state electrolytes and solid polymer electrolytes (SPEs) [9]. Although the ionic conductivity in an inorganic solid-state electrolyte is comparable to that of conventional liquid electrolytes, its brittle nature and high electrode/electrolyte interface impedance are likely to preclude large-scale applications [10,11]. On the other hand, SPEs have low flammability, good flexibility and safety, and provide stable contact between electrode and electrolyte, which are well suited for large-scale processing [12,13]. However, the well-known problems of SPEs are their relatively low ionic conductivity and short cycle life, which result in low capacity utilization and rapid deterioration of performance [14]. Therefore, achieving fast ion transport and stable cycle stability in SPEs remains to be main practical interest, and is also fundamentally challenging due to the elusive interaction between the electrolyte and Li^+ transport [15].

Within the myriad of available SPE materials, poly(ethylene oxide) (PEO) as a versatile polymer, has distinct advantages such as excellent mechanical properties and compatibility with lithium salts [16]. In particular, PEO has good chain flexibility and unique ether-oxygen linkages. The oxygen atoms in PEO chains are good electron donors with suitable interatomic separation and can wrap around Li^+ to form multiple intra-polymer bonds. The low barriers to bond rotation allow segmental motion of the PEO chain, providing a driving force for Li^+ transport [17]. Unfortunately, the dominant crystalline domains in

* Corresponding author.
** Corresponding author.
E-mail addresses: baigang73@126.com (B. An), fli@imr.ac.cn (F. Li).

https://doi.org/10.1016/j.nanoen.2020.104976
Received 30 March 2020; Received in revised form 17 May 2020; Accepted 17 May 2020
Available online 27 May 2020

semi-crystalline PEO dramatically hamper the mobility of Li^+ through the electrolyte [18,19]. Several approaches have been developed in recent years to decrease the crystallinity or lower the melting point by chemical and physical methods including copolymerization, cross-linking of PEO macromers and blending PEO with inorganic substances [20–25]. High ionic conductivity and electrochemical stability have been achieved together with low crystallinity for the modified PEO [26]. However, the modified PEO-based electrolytes still require a working temperature ranging from 60 to 90 °C because of its poor Li^+ conductivity and low transference number at low temperatures (<60 °C), especially at a high cycling rate. Therefore, the number of cycles and rate capability are far below what is needed for practical applications.

Lithium polysulfides are intermediate reaction species generated from a sulfur cathode into electrolytes during the charge/discharge of lithium sulfur batteries [27,28]. The polysulfide-shuttling effect is caused by the dissolution and diffusion of polysulfide anions in electrolytes [29]. The dissolved polysulfide anions have a good ability to migrate towards the Li anode. Another remarkable feature of lithium polysulfides is their inherent fast ionic conduction due to the high polarizability of sulfide ions weakening the interaction between the anions and the lithium ions [30,31]. Considering these unique properties of polysulfides and PEO, the intention of our research is to take full advantage of them to maximize ionic conduction in solid-state PEO--based electrolytes. A chemically stable sulfur-bridged complex (abbreviated as S-PEGMA) was prepared by the direct copolymerization of elemental sulfur with poly(ethylene glycol) methacrylate (PEGMA) monomers inspired by inverse vulcanization [32]. An all-solid-state LIB was formed by combining S-PEGMA with PEO and LiTFSI as a solid electrolyte separator (abbreviated as ScPEO), and $LiFePO_4$ and Li as electrode materials. In order to obtain fast Li^+ transport in the solid electrolyte, the solid-state electrolyte membrane was activated *in situ* by the electrochemical activation of ScPEO with a limiting terminal voltage between 1.7 and 2.3 V, leading to the formation of organic lithium polysulfides. The grafting of organic lithium polysulfides (-RS_nLi, R = poly(ethylene glycol) methacrylate chain) onto the PEO chain has achieved fast Li^+ transport and intimate electrode-electrolyte interface, which results in the dendrite-free Li-metal deposition and a long cycle life in the cell.

2. Results and discussion

Fig. 1 illustrates the detail stepwise procedure for the fabrication of lithium polysulfide grafted PEO-based solid polymer electrolytes. A certain amount of PEGMA and sulfur powder was mixed together in a sealed glass bottle, and then heated to 185 °C for 2 h. After cooling to room temperature, a sulfur-bridged PEGMA copolymer was obtained as the solid-electrolyte precursor (S-PEGMA). To highlight the "sulfur-bridge" containing the long sulfur-sulfur bond, the S-PEGMA was dissolved in chloroform and left standing for a week. Solution-grown single crystals of *cyclo*-S_8 were produced as determined by single-crystal X-ray diffraction analysis (Fig. S1). These results indicate that S atoms could detach from the sulfur-bridged copolymer by breaking weak S–S bonds in long-chain polysulfides. The next and key step is to promote the conversion of S-PEGMA to organic lithium polysulfides using an electrochemical method based on the formation of polysulfides in lithium sulfur batteries. Composite electrolyte solutions were created by directly mixing lithium bis(trifluoromethanesulfonyl)imide (LiTFSI), S-PEGMA and PEO in an acetonitrile solution. After evaporation, solid ScPEO electrolyte membranes were obtained with a bright yellow color (The image in Fig. 1). In a Li|ScPEO|$LiFePO_4$ cell, the activation process involves the chemical reduction of the solid phase. 10 cycles with a terminal voltage ranging from 1.7 to 2.3 V (vs. Li^+/Li) were aimed at breaking the long "sulfur-bridge" into short polysulfide chains. Another 10 cycles with a higher terminal voltage from 2.5 to 4.2 V (vs. Li^+/Li) implanted enough Li^+ into the electrolytes and promoted structural interaction between the polysulfides and the PEO chains. During this process, the color of the electrolyte membrane changed from yellow to blood-red (Fig. 1). Generally, the characteristic color of lithium polysulfides (Li_2S_n, $1 \le n \le 8$) changes from white (Li_2S) to yellow (Li_2S_n, n = 2, 3) to blood-red (Li_2S_n, $4 \le n \le 8$) as the S–S chain length increases [33], hence, we conclude that the S–S chain of the generated lithium polysulfides in the solid electrolyte membrane should contain four to eight sulfur atoms.

In order to prove that the generated polysulfide anions were grafted onto the vinyl-terminal of PEGMA chain, rather than existing in the polymer matrix, proton nuclear magnetic resonance spectroscopy (^1H NMR) was used to examine the electrolytes before and after activation. Fig. 2a shows the ^1H NMR spectra of PEGMA. The chemical shifts at 6.1 and 5.6 ppm are attributed to the protons in the CH_2=C groups of

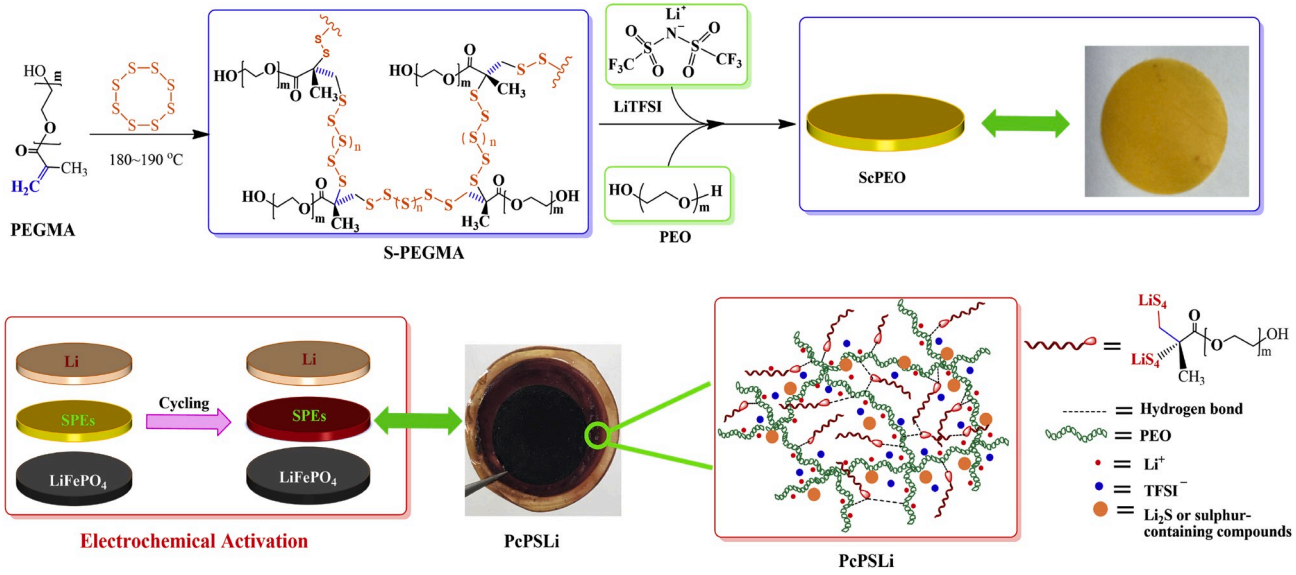

Fig. 1. Schematic showing the fabrication of lithium polysulfide grafted solid-state electrolytes. The optical images are also provided. The yellow membrane is the pristine solid-state electrolyte. After activation, a color change of the electrolyte membrane from yellow to blood-red is clearly visible. The lower right diagram is a representation of the materials and their interactions in PcPSLi.

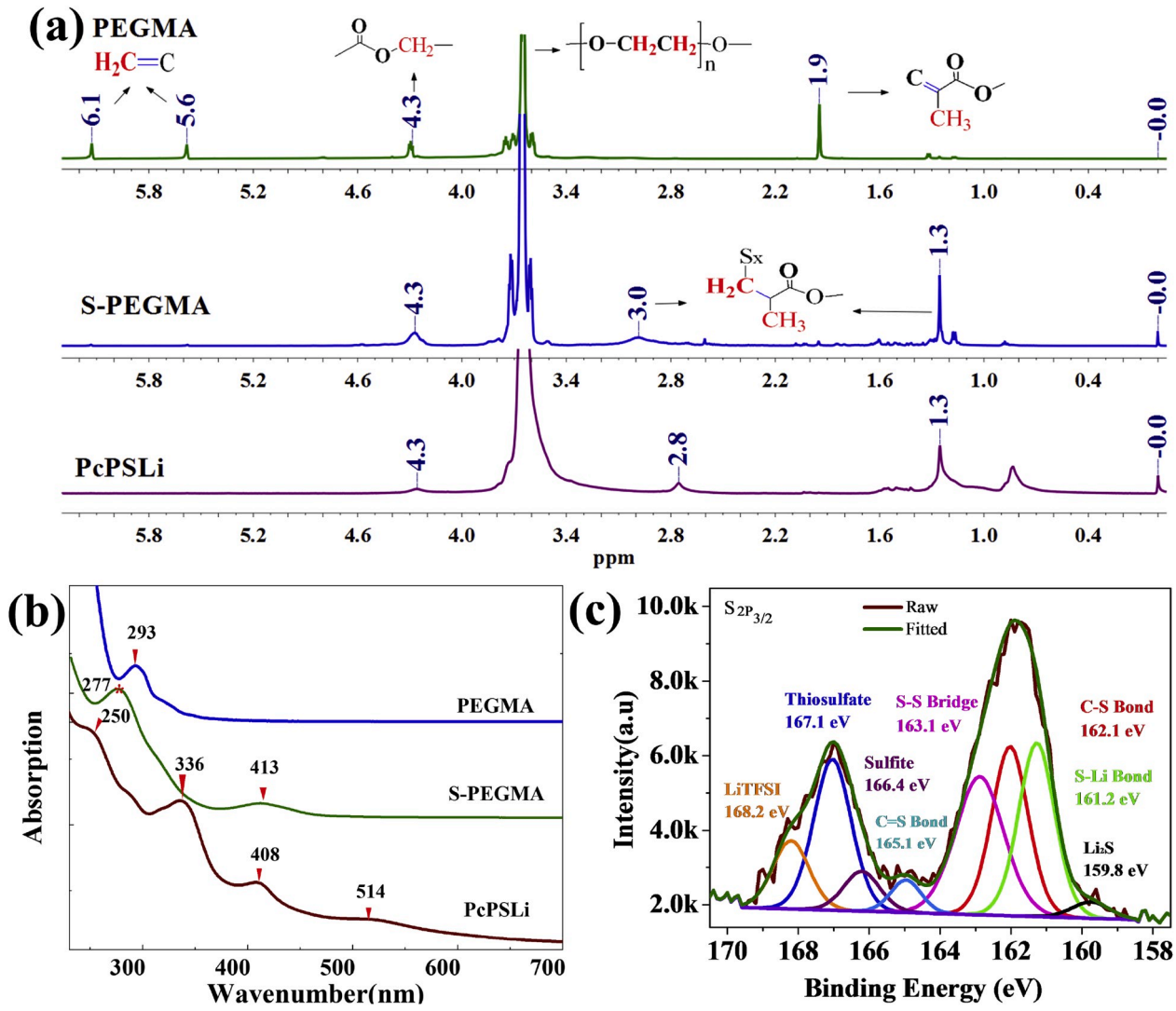

Fig. 2. Characterization of the electrolyte. (a) ^{1}H NMR spectra of PEGMA, S-PEGMA and the activated electrolyte (PcPSLi) measured in $CDCl_3$. (b) UV–vis spectra of PEGMA, S-PEGMA and PcPSLi measured in a CH_3CN solution. (c) High-resolution S2p3/2 XPS spectrum of PcPSLi.

PEGMA. The grafting of the long "sulfur-bridge" to the vinyl-terminal of PEGMA has resulted in the appearance of chemical shift at 3.0 ppm, due to the transformation of the CH_2═C group to –SCH_2-C. After activation, the peaks from the protons in CH_2═C groups disappear, and the resonance peak (-SCH_2-C) shifts slightly to a lower magnetic field at 2.8 ppm, which is associated with the reduction of the "sulfur-bridge". These results demonstrate that the polysulfides are attached to the PEGMA chains, and electrochemical reduction of the sulfur-bridged copolymer is incapable of causing cleavage of the C–S bond. Furthermore, the peaks at 3.5–3.8 ppm arise from the protons in –OCH_2CH_2O- and peak splitting is clearly observed in PEGMA and S-PEGMA because of the spin-spin coupling of each proton with two adjacent hydrogen atoms. However, in the activated electrolytes, no prominent coupling was observed. This unexpected finding suggests that polysulfide anions form a strong interaction with the hydrogen in the –OCH_2CH_2O- units of PEO by hydrogen bonding interaction (-S···H), disturbing the transmission of electrons moving from protons to protons in –OCH_2CH_2O- and weakening the spin-spin interaction.

To further determine the n value of -RS_nLi in the activated electrolytes, UV–visible spectroscopy (UV–vis) and X-ray photoelectron spectroscopy (XPS) were used to characterize the generated polysulfide species in the solid electrolytes. Fig. 2b shows the UV–vis spectra of the solid electrolytes induced by the structural change in PEGMA. A moderate absorption peak at 293 nm is related to the methacrylate group, and after copolymerization with sulfur the two absorption peaks at 277 and 413 nm can be assigned to long polysulfide chains, which is in agreement with reports that the typical absorption peaks of the S_x^{2-} ($4 \leq x \leq 8$) chain are detected at around 270–280 nm and 400–620 nm [34,35]. The peak between 400 and 620 nm is indicative of the polysulfide order, with the peak moving from 470 to 580 nm as the value of x increases from 4 to 8. According to the literature [36,37], the UV–visible spectrum of the activated electrolytes (PcPSLi) produced after the electrochemical reduction of ScPEO indicates the formation of polysulfide chains with four representative absorption peaks near 250, 336, 408 and 514 nm, which is consistent with the S_4^{2-} band. We concluded that the n value of -RSnLi should be approximate –RS_4Li group. The conversion of a long sulfur-bridge to the corresponding –RS_4Li grafted on PEGMA should be reasonable in solid electrolytes due to the moderate length S–S chain and its relative stability in the disproportionation reaction of Li_2S_n ($1 \leq n \leq 8$) [38]. Fig. 2c shows XPS results for the S (2p3/2) region with two S-related chemical bonds of the activated electrolyte identifiable: an S–C bond (162.1 eV) and an S–S bond (163.2 eV), which agree well with the organic sulfide-type state of sulfur in polymer-capped sulfur copolymers [39,40]. In contrast to the original ScPEO electrolytes (Fig. S2), the expected peaks are present in the activated electrolytes, with a major peak at 161.2 eV for terminal sulfur

which is assigned to the S–Li band in $–S_4Li$. Two peaks at 159.8 and 166.4 eV are observed for sulfur-containing compounds and are assigned to the formation of Li_2S or $–CS_2Li$, and thiosulfate, respectively [41,42]. The presence of such peaks in the activated electrolytes indicates that the electrochemical reduction of a long sulfur-bridge to $–S_4Li$ results in additional products incorporated in the PEO network.

Theoretical calculations are also helpful in understanding the reactions between an S_8 ring and PEGMA, and the formation of $-RS_nLi$. We have constructed a hydroxyethyl methacrylate [HEMC, $HOCH_2CH_2OC(=O)C(CH_3) = CH_2$)] monomer as one repeat unit linking PEO to methacrylic acid. Fig. 3a and b indicate four possible structures in the models. One is that two terminal S atoms bond with the C_α atom of a HEMC monomer and the C_β atom of another HEMC monomer. The other three modes are that two terminal S atoms bond with the C_α and C_β atoms of the same HEMC monomer, or with two C_α (C_β) atoms of different PEO monomers (Fig. S3). Of these four possible modes, we found that two terminal S atoms bonding with the C_α and C_β atoms of the same HEMC monomer is energetically unfavorable with a small positive ΔH of +0.018 eV, while other three modes show almost the same negative ΔH, ranging from −1.588 to −1.655 eV. This means that these three modes are all possible during the cross-linking reaction between HEMC and S_8. Considering the similarity (one S_8 connects with two HEMC monomers) of the ΔH values of these three modes, we only consider the case with the lowest ΔH of −1.655 eV (Fig.3b). Fig. 3c and d respectively show the isosurface plots of the highest occupied molecular orbital (HOMO) and the lowest unoccupied molecular orbital (LUMO) of the considered HEMC/S_8 cross-linking product. Obviously, the HOMO is mainly contributed by the C–S and S–S bonds, and the LUMO is mainly located at the central five S–S bonds of the chain produced by opening the S_8 ring. This result implies that one of these five central S–S bonds may break and form three possible products HEMC-S_2Li/HEMC-S_6Li, HEMC-S_3Li/HEMC-S_5Li, or HEMC-S_4Li/HEMC-S_4Li after lithiation. In order to identify the most energetically favorable product, we further calculated the energy change (ΔE) for the lithiation reaction of HEMC/S_8. As shown in Fig. 3e–g, the energy changes (ΔE) of the three possible lithiation reactions of HEMC/S_8 were calculated to be −1.122, −1.428, and −2.102 eV for the three lithiation products HEMC-S_2Li/HEMC-S_6Li, HEMC-S_3Li/HEMC-S_5Li and HEMC-S_4Li/HEMC-S_4Li, respectively. Therefore, it is concluded that HEMC-S_4Li/HEMC-S_4Li is the most energetically favorable product after the lithiation of HEMC/S_8, which is consistent with our experiment results.

As far as PEO-based electrolytes are concerned, a high ionic conductivity generally requires low crystallinity and more segmental motions of the polymer chains. To understand the effect of chemical structure on the physical properties, the crystallinity of sulfur, the reference ScPEO electrolyte and the activated electrolyte (PcPSLi) were evaluated by X-ray diffraction (XRD) (Fig. S4). The XRD pattern of the PEO-related membranes show two intense characteristic peaks near 2θ = 19.1° and 23.3°, corresponding to the crystalline phase of PEO. XRD analysis on the same region of the ScPEO membranes was carried out to compare the crystallinity before and after electrochemical activation. The peak intensity of PEO decreased after activation, and the peak at 19° was slightly shifted to 19.2°. The change reflects the fact that $–RS_4Li$ was formed at the same time as the PEO crystallinity was reduced, and interaction occurred spontaneously between the ether oxygen of the PEO network chains and the $–RS_4Li$. Based on the XRD data, the crystallinity was calculated to be 29.7% for ScPEO and 22.5% for PcPSLi. The reduced crystallinity of the electrolyte is generally associated with an increased content of the amorphous phase that is beneficial to Li^+ transport. This can also be concluded from the changes in the differential scanning calorimetry thermograms (DSC) of the PEO-related films. Plots of glass transition temperatures (T_g) for PEO, ScPEO and PcPSLi are given in Fig. S5, showing that it shifts from −56 °C to −39 °C. The increased T_g implies the formation of a complex molecular network due to the strong ion dipole interaction between the dissociated Li^+ and the generated organic polysulfide anions, and the PEO network chains [43]. SEM images show the surface morphology of the pristine ScPEO, indicating a rough surface with micro-wrinkles found in the crystalline domains (Fig. 4a). In contrast, the activated electrolyte is distinctly smooth and homogenous (Fig. 4b). The elemental maps of fluorine and sulfur suggest that these elements are uniformly dispersed in the SPEs. In addition, the thermal stability of the SPEs also plays a critical role in battery safety during cell operation. The activated electrolyte PcPSLi remains relatively stable until 210 °C due to the interaction between the $–RS_4Li$ and the PEO chains (Fig. 4c and d). Two weight loss steps can be distinguished in the TG curve. The first between 210 and 350 °C is attributed to the condensation of polysulfides and is higher than that for S_8 decomposition (near 180 °C) [44]. The second weight loss begins at

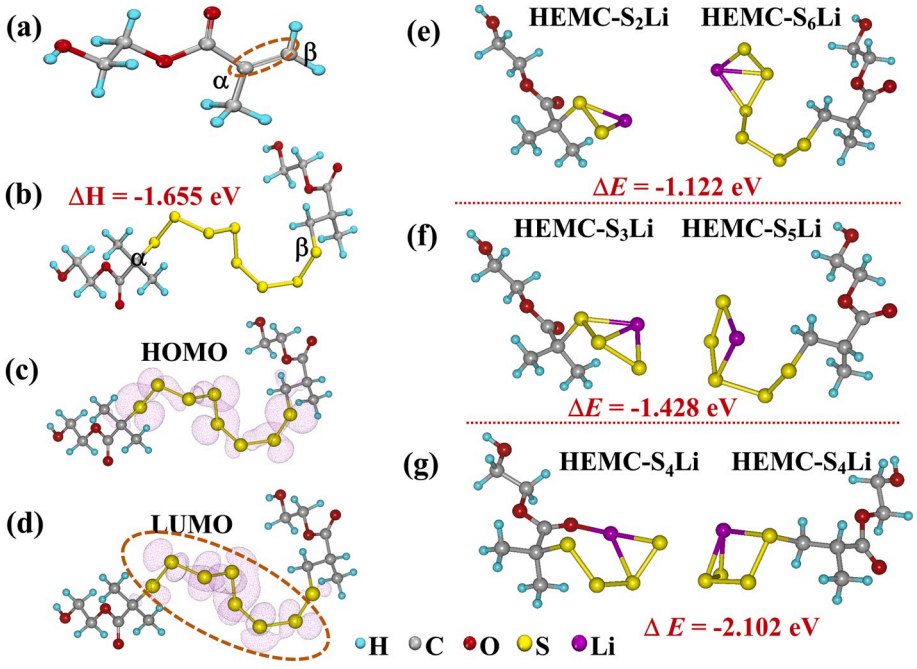

Fig. 3. Schematic of structural models and calculations of energy changes of the product structures by density functional theory. (a) Structure of the HEMC monomer. (b) HEMC/S_8 cross-linked product. (c) and (d) the isosurface plots of the HOMO and LUMO of the HEMC/S_8 cross-linked product. The C–C double bond and the LUMO distribution pattern are marked by dashed blue ellipses. The two C atoms forming the C–C double bond of PEO are labled α and β, respectively. The cross-linking reaction enthalpy (ΔH) between two HEMC monomers and an S_8 ring molecule is presented. The isosurface level is 0.002 e/Å^3 for both the HOMO and LUMO. (e–g) schematic structures of three possible lithiation products of HEMC/S_8. The corresponding energy changes (ΔE) are also shown.

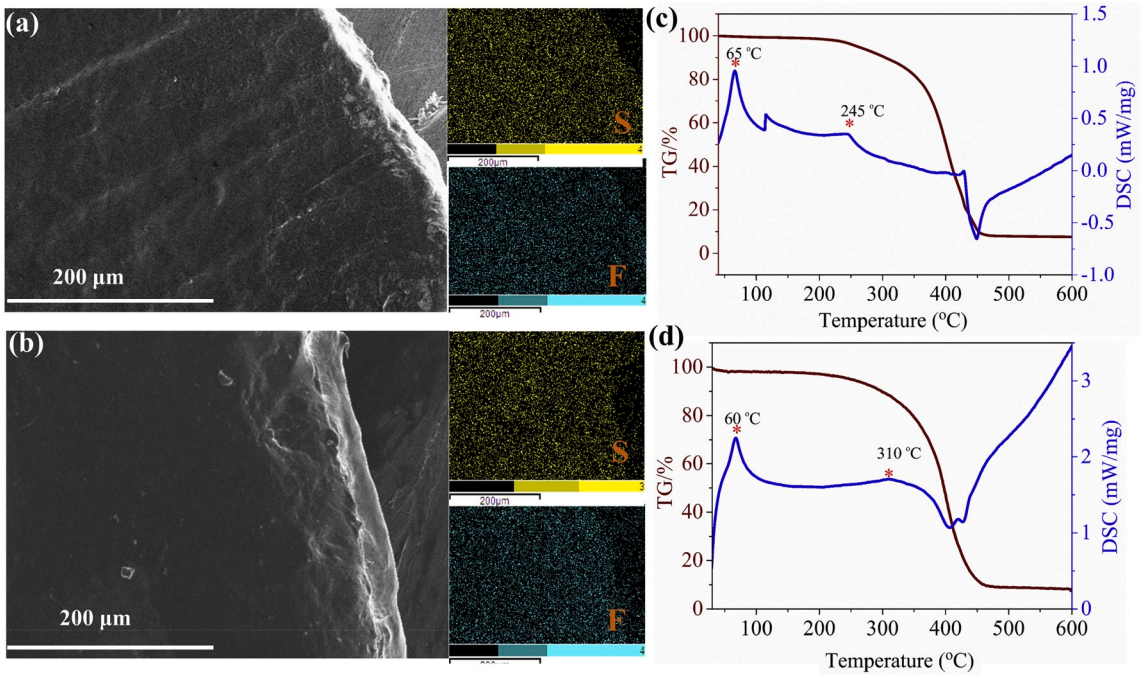

Fig. 4. Physical properties. (a) SEM image and EDS elemental mappings of ScPEO. (b) SEM image and EDS elemental mappings of PcPSLi. (c) TG-DSC thermogram of ScPEO. (d) TG-DSC thermogram of PcPSLi.

around 350 °C and is caused by degradation of the polymer backbone.

The electrochemical stability, ionic conductivity and transference number are the most fundamental parameters for evaluating solid-state electrolytes. Fig. 5a shows linear sweep voltammetry (LSV) scans before and after activation of the ScPEO membrane run on a S|electrolyte|Li cell. A very low background current was measured in the potential range of 2.0 to 6.5 V (vs Li^+/Li) at room temperature, whereas the current began to obviously increase when the potential exceeded 4.5 V for ScPEO and 5.4 V for the activated PcPSLi. This significant increase of 0.9 V indicates that a strong interaction between the polysulfide ions and the PEO chains broadened the electrochemically stable window of the solid polymer electrolyte. The wide range of oxidation potentials allows the use of PcPSLi as a solid electrolyte in a high potential lithium battery. We also performed electrochemical impedance spectroscopy (EIS) analysis of the ScPEO membrane before and after activation in the temperature range of 293 K to 343 K. In the EIS curves (Fig. S6), a complex impedance plot for T < 313 K shows a half circle followed by a sloping line, but when the temperature goes above this value only a sloping line is observed. This phenomenon is attributed to the liquid-like environment of charge carriers, which allows fast dielectric relaxation and prevents dielectric capacitance throughout the material [45,46]. Conductivities calculated from the EIS curves show that the activated electrolyte has a conductivity of $7.1*10^{-6}$ S/cm at 298 K, which is 3 times that of the pristine membrane ($2.37*10^{-6}$ S/cm), but at 323 K, a dramatic increase in conductivity is found for the activated PcPSLi membrane. It reaches ~$2.13*10^{-4}$ S/cm, which is about one order of magnitude higher than that of the unactivated membrane ($2.17*10^{-5}$ S/cm). We also compared the PcPSLi with the results from the literatures for ionic conductivity of PEO electrolyte, the –RS_4Li-grafted PEO-based electrolytes is comparable to that of known PEO-based electrolytes at higher temperatures (Table S1 and Fig. S7) and the reported covalent organic frameworks ($2.13*10^{-4}$ S/cm at 70 °C) [47].

Fig. 5b shows the temperature dependence of the conductivity of the pristine and activated electrolytes. Arrhenius plots of the ionic conductivity show a slightly off-linear behavior over the temperature range probed (from 293 to 343 K). However, the ionic conductivity was found to increase with increasing temperature. When polysulfide anions were grafted on the PEO chains, the ionic conductivity was greatly increased, which is explained by the obvious increase in the number of coordinating sites, local structural relaxations and the motions of the polymer chain segments coordinated with Li^+ [48,49]. The polysulfide anions attached to the ends of the PEO chains can increase the number of interaction sites between the PEO chains, resulting in an increase in the amount of amorphous material [50]. The terminal polysulfide chains can also increase the activity of Li^+ accompanied by segmental motion of the PEO chains. It is also important to note that the Li^+ transference number (t_+) of the activated electrolyte was measured to be ~0.61 (Fig. 5c), which is much higher than that of the reported values for pure PEO which are between 0.2 and 0.5 [51]. The t_+ values of pure PEO and ScPEO electrolytes were also measured under the same conditions, with values of 0.28 and less than 0.1, respectively (Figs. S8 and 9). Li^+ transport was significantly improved by the conversion of the long sulfur-bridge in ScPEO to the corresponding organic lithium polysulfides in PcPSLi. As a result, the ionic conductivity of the activated electrolyte reaches $2.13*10^{-4}$ S/cm at 50 °C with a Li^+ transference number of ~0.61, which should be enough for a lithium battery test.

To gain insight into the positive effect of lithium polysulfides on electrochemical performance, all-solid state $LiFePO_4$|ScPEO|Li cells were assembled and cycled at 50 °C. As mentioned above, the primary step is to activate the solid-state electrolyte by multiple charge/discharge cycles, which is regarded as the "*in-situ* electrochemical activation process". Fig. 5d shows the first ten galvanostatic charge and discharge curves for such a cell measured between 1.7 and 2.3 V at 0.2 C, followed quickly by the second ten galvanostatic charge and discharge curves with voltages ranging from 2.5 to 4.2 V at 0.2 C. The first charge-discharge platform belongs to the lithium-sulfur reaction [52], which promote the formation of the polysulfide anion-lithium complex (-RS_4Li), and the second belongs to the $LiFePO_4$ battery, which makes the electrolyte film more stable and sufficient Li^+. As observed from the first ten galvanostatic charge and discharge curves, the discharge capacity of the $LiFePO_4$|ScPEO|Li cell tends to show rapid capacity fade and charging is difficult, indicating that charging and discharging are completely irreversible. The typical characteristics of a Li–S battery (the illustration in Fig. 5d) have an initial voltage region of 2.1–2.4 V that is

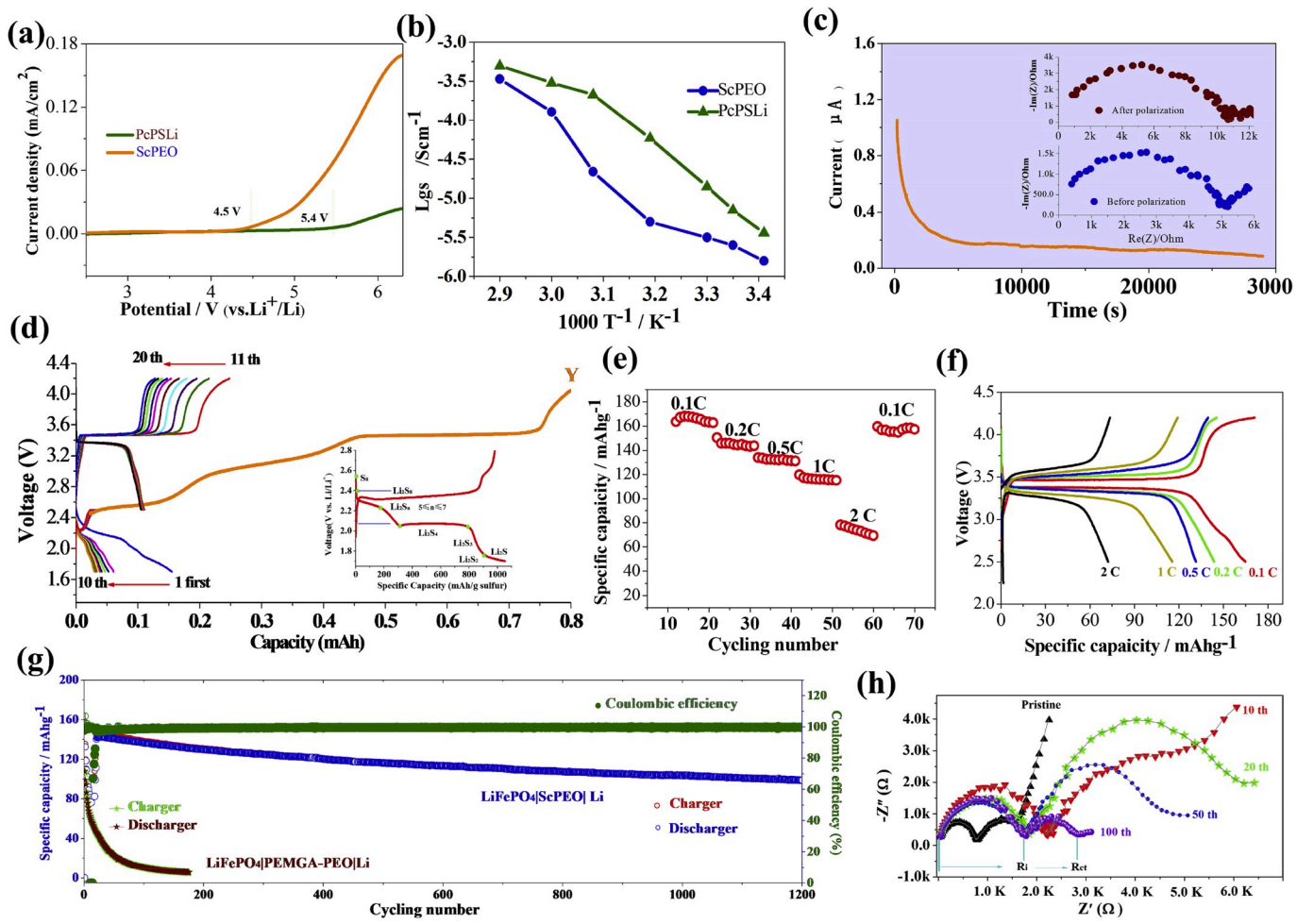

Fig. 5. Electrochemical properties. (a) LSV of the ScPEO electrolyte and the activated PcPSLi electrolyte at room temperature. (b) The temperature dependence of ionic conductivity. (c) The Li|PcPSLi|Li symmetrical cell under a polarization voltage of 10 mV. The corresponding EISs before and after the polarization are shown in the insets. (d) Charge/discharge profiles of the $LiFePO_4$|ScPEO|Li cell during the activation process (vs. Li/Li^+), and the bold orange curve Y indicates that the activation process changed from stage one to stage two accompanied by a voltage change from 2.5 to 4.2 V. (e) C-rate capability of the $LiFePO_4$|ScPEO|Li cell after activation. (f) Charge-discharge voltage profiles of the $LiFePO_4$|ScPEO|Li cell with various rates after activation. (g) Long-cycle performance of all-solid-state $LiFePO_4$|ScPEO| Li and $LiFePO_4$|PEMGA-PEO|Li cells operated at 1 C. (h) EISs of the $LiFePO_4$|SCPEO|Li cell after 20, 50 and 100 cycles at room temperature.

assigned to the reaction of S_8 to Li_2S_x ($4 \leq X \leq 8$) [53]. In comparison, the plateau between 2.1 and 2.3 V in a $LiFePO_4$|ScPEO|Li cell corresponds to the transformation of polysulfides to $-RS_4Li$, and the discharging capacity gradually fades with the cycling. This phenomenon is in good agreement with the irreversible process of the reduction of long sulfur bridges to $-RS_4Li$. As shown in Fig. 5d (the bold orange curve Y), when the voltage changed from 2.5 to 4.2 V, the first charging process is somewhat slow because the migration of Li^+ from the cathode to solid electrolytes needs go through the activation process. The second activation process is clearly distinguished from the first, in which the discharge cycles are stable, and charge capacity gradually fades until the charge/discharge efficiency becomes balanced and totally corresponds to the reversible cycles in a liquid $LiFePO_4$ battery.

After activation, Fig. 5e and f shows charge/discharge curves of the cell at different rates at 50 °C. The $LiFePO_4$|PcPSLi|Li cell offers a high discharge capacity of 165 mA h g^{-1} at 0.1 C, approaching 97.1% of the theoretical value, which is comparable to liquid $LiFePO_4$ electrolytes. As the current density increases, the all-solid-state battery still delivers high discharge capacities of 145, 132, 115 and 71 mA h g^{-1} at 0.2, 0.5, 1, and 2 C, respectively, comparable to or better than similar polymer electrolyte systems or hybrid organic-inorganic electrolyte materials at higher temperatures (≥55 °C) [54,55]. When the current density was returned to 0.1 C, the capacity retention of the $LiFePO_4$|PcPSLi|Li cell was close to 95.1% of the initial discharge capacity at 0.1 C, indicative of the robust and stable PcPSLi electrolyte in the battery. To evaluate cycle life, a long cycling test was first performed at a high rate of 2 C (Fig. S10). In the first 20 cycles, the cell was subjected to the activation stage, and both charge capacity and Coulombic efficiency became unstable. Subsequently, the current rate was set to 2 C and a high discharge specific capacity (92.6 mA h g^{-1}) was achieved, with the corresponding charge capacity being slightly higher than the discharge capacity. The reason can be explained that the activation process is not sufficient at a high current density. Another ten cycles were required to improve the solid electrolyte stability, while the Coulombic efficiency of the cell increased from 92.3% to 97.3%. After 1200 cycles, the capacity dropped at the 2 C rate to ~53.6 mA h g^{-1}, corresponding to a 42.1% loss of the original capacity. It is obvious that the capacity of this solid-state lithium metal battery still drops considerably for high discharge rates as it does in a liquid electrolyte system. When the cell was used at 1 C, an initial discharge capacity of 140.4 mA h g^{-1} was achieved (Fig. 5g). After 1200 cycles, the cell still delivered a high capacity of 100.3 mA h g^{-1} and the Coulombic efficiency was close to 100%. The capacity decay rate was as low as 0.024% per cycle, indicating the $LiFePO_4$|PcPSLi|Li cell with the solid electrolyte shows high cycling stability. The conventional $LiFePO_4$|PEMGA-PEO|Li cell delivered only an initial capacity of about 70 mA h g^{-1} at 1 C and deteriorated after tens of cycles at 50 °C (Fig. 5g). The

superior cycling stability of the $LiFePO_4$|PcPSLi|Li cell indicates that –RS_4Li is the decisive factor for fabricating stable electrolyte-electrode interfaces and effectively suppressing Li dendrite formation. To gain a better understanding of the electrolyte-electrode interface changes caused by –RS_4Li, EIS was used to measure the internal resistance of the cell during charge-discharge cycles. As shown in Fig. 5h and the equivalent circuit (Fig. S11), the EIS of the pristine cell is composed of two partial semicircles and a straight sloping line at low frequencies. The first semicircle at the high-frequency region reflects the interface resistance (R_i) of the solid-state interface layer formed on the surface of the electrodes, while the second semicircle at medium frequencies is attributed to the charge transfer resistance (R_{ct}) [56]. During the activation stage, the cell exhibited both R_i and Rct increases as the number of cycles increased, but the R_i shows negligible changes in the subsequent 100 cycles. This suggests that the interface between the solid electrolyte and the electrodes undergoes a process from the interface formation to steadiness during the charge/discharge cycles. The value of R_{ct} decreased significantly from the 20th to the 120th cycle, reflecting the positive kinetics of the cell reaction. The stable R_i and decreasing R_{ct} indicate the relatively stable and robust contact between the electrolyte and the electrodes [57].

To further gain insight into the effect of the solid-state polymer electrolyte on the performance of battery, the surface morphologies of the electrolyte membrane, $LiFePO_4$ cathode and lithium anode from a disassembled $LiFePO_4$|ScPEO|Li cell after 150 charge/discharge cycles were examined by SEM (Fig. 6a–f). Compared with the initial surface of the $LiFePO_4$ cathode, the surface after cycling was found to be infused with a thick layer of solid polymer electrolyte, and the surface of the lithium metal electrode was a smooth and homogeneous layer without any lithium dendrites. The maintaining of good cyclic stability and reversible capacity could be explained by the thick layer produced between electrolyte and electrode, promoting electrolyte-electrode interfacial contact and forming stable and compatible electrode interfaces. The good contact at the interface between the $LiFePO_4$ and electrolyte membrane is further substantiated by data regarding cross-sectional SEM image and the elemental mapping of S and F as displayed in Fig. 6g–i. This improvement is basically the result of organic polysulfide anions, which not only increase the interaction between the polymer structures but construct interfacial layers suitable for Li^+ transport [58], thus improving the PEO-based electrolyte performance. The smooth and homogeneous PcPSLi electrolyte membranes after cycling are also beneficial for uniform lithium deposition/stripping.

3. Conclusions

In summary, inspired by the shuttling effect of polysulfide anions, we designed and fabricated the lithium polysulfides-grafted PEO-based electrolytes by the in-situ reduction of the copolymers of sulfur reacting with PEGMA. These electrolytes have a high ionic conductivity (2.13 $*10^{-4}$ S/cm at 50 °C) and Li^+ transference number (~0.61). Compared with the pure PEO-based electrolytes, the incorporation of PcPSLi electrolytes in the $LiFePO_4$ battery dramatically increases the rate capacity and cycle stability. These significant performance improvements can be attributed to the strong interaction between the PEO chains and organic polysulfide anions and the formation of stable electrolyte-electrode layers. The polysulfide anions grafted on the vinyl-terminal of the PEGMA chains increase the terminal segmental motion of the PEO chains and loosen the O–Li^+ coordination, thus achieving much faster Li^+ transport than in PEO. This contribution demonstrates that organic polysulfide anions can be used as promising polymer electrolytes to enable rapid Li^+ transport and improve interface stability and endow all-solid-state polymer lithium batteries with a long cycle life.

4. Experimental section

4.1. Preparation of the solid polymer electrolyte

Poly(ethylene glycol) methacrylate (PEGMA) and sulfur powders

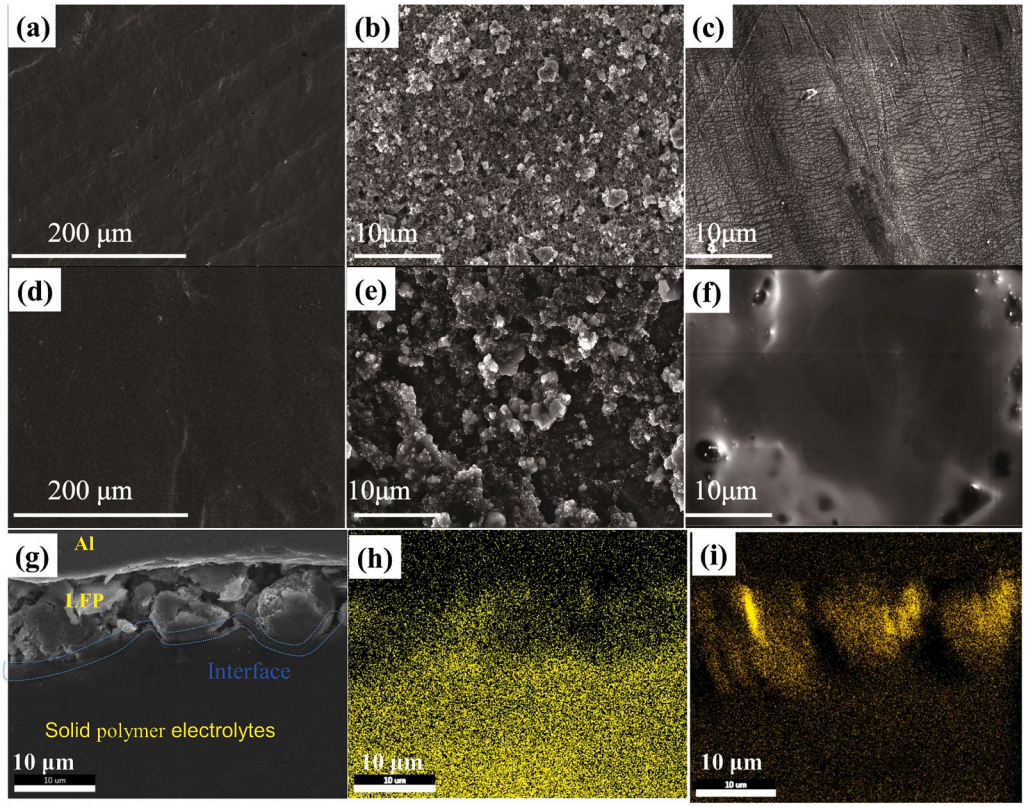

Fig. 6. Surface morphology images of all-solid polymer $LiFePO_4$ cells. (a) ScPEO electrolyte membrane. (b) Pristine $LiFePO_4$ cathode. (c) Pristine lithium metal foil. (d) PcPSLi electrolyte membrane. (e) $LiFePO_4$ cathode after 150 cycles at 0.5 C and 50 °C. (f) Lithium metal foil after 150 cycles at 0.5 C and 50 °C. (g) The cross-sectional SEM image and the corresponding elemental mappings of the interface between $LiFePO_4$ cathode and electrolyte after activation, EDS elemental maps of S (h) and F (i).

were mixed together in a ratio of 10:1 under stirring, then heated 185 °C for 2 h. As the mixture was cooled to room temperature, a viscous orange liquid was obtained. According to the structure characteristic, the viscous orange polymer is regarded as the sulfur-bridged poly(ethylene glycol) methacrylate, which is abbreviated as S-PEGMA. Subsequently, a large amount of PEO and LiTFSI (EO/Li = 16/1 in molar ratio) dissolved in 40 mL of CH_3CN was stirred, and a mass of S-PEGMA equal to the weight of the PEO was added to the solution. The mixture was continuously stirred at room temperature for 12 h to obtain a yellow viscous solution. The S-PEGMA-PEO-LiTFSI mixture was then poured into a polytetrafluoroethylene mould and dried in a vacuum oven at 50 °C for 36 h. Finally, the dry electrolyte membrane was obtained and marked as ScPEO. As a comparison, sulfur-free PEGMA-PEO-LiTFSI membranes were also fabricated under the same conditions.

4.2. Electrode preparation and battery assembly

The cathode was fabricated with $LiFePO_4$ as the active material, Super P as the conductive additive, and both poly(vinylidene fluoride) (PVDF) and the above polymer electrolytes as the binders, where the weight ratio of $LiFePO_4$/Super P/PVDF/ScPEO was around 75/15/5/5. A prepared slurry in NMP was cast on a carbon-coated aluminum current collector. Circular electrodes with an average $LiFePO_4$ mass loading of 0.8–1.2 mg were used as the working electrodes. For the assembly of the all-solid-state LIBs, lithium metal foil was used directly as the anode. The thickness of the electrolyte membranes for battery tests was between 70 and 90 μm. In order to test the ionic conductivity and Li^+ transference number during the activation process, electrolyte membranes with a thickness over 150 μm were easy to strip manually from electrodes and re-assemble in Li–Li or S–S symmetrical cells.

Declaration of competing interest

The authors declare no competing financial interest.

CRediT authorship contribution statement

Chengguo Sun: Writing - original draft, Data curation. **Zhenxing Wang:** Data curation, Formal analysis. **Lichang Yin:** Methodology, Writing - original draft. **Shengjun Xu:** Investigation, Validation. **Zahid Ali Ghazi:** Investigation. **Ying Shi:** Conceptualization, Visualization. **Baigang An:** Supervision. **Zhenhua Sun:** Validation, Visualization. **Hui-Ming Cheng:** Writing - review & editing. **Feng Li:** Supervision, Funding acquisition, Validation.

Acknowledgements

The authors acknowledge financial support from the National Natural Science Foundation of China (51525206, 51521091, 51672118, 21701077, 11972178, 51472249), Talent Project of Revitalizing LiaoNing (XLYC1807114, 2019LNZD01), MOST (2016YFA0200102, 2016YFB0100100), the China Postdoctoral Science Foundation (2016M601353), the Key Research Program of the Chinese Academy of Sciences (KGZD-EW-T06), Liaoning Key Laboratory of Energy Materials and Eectrochemistry and the CAS/SAFEA International Partnership Program for Creative Research Teams. The theoretical calculations in this work were performed on TianHe-1(A) at National Supercomputer Center in Tianjing and Tianhe-2 at National Supercomputer Center in Guangzhou.

Appendix A. Supplementary data

Supplementary data to this article can be found online at https://doi.org/10.1016/j.nanoen.2020.104976.

References

[1] J. Woods, N. Bhattarai, P. Chapagain, Y. Yang, S. Neupane, Nano Energy 56 (2019) 619–640.
[2] Y.-S. Lee, J.H. Lee, J.-A. Choi, W.Y. Yoon, D.-W. Kim, Adv. Funct. Mater. 23 (2013) 1019.
[3] W. Zhang, J. Nie, F. Li, Z.L. Wang, C. Sun, Nano Energy 45 (2018) 413–419.
[4] Y. Yuan, J. Lu, Carbon Energy 1 (2019) 8–12.
[5] X.Y. Tao, Y.Y. Liu, W. Liu, G.M. Zhou, J. Zhao, D.C. Lin, C.X. Zu, O.W. Sheng, W. K. Zhang, H.W. Lee, Y. Cui, Nano Lett. 17 (2017) 2967–2972.
[6] C. Wang, L. Zhang, H. Xie, G. Pastel, J. Dai, Y. Gong, B. Liu, E.D. Wachsman, L. Hu, Nano Energy 50 (2018) 393–400.
[7] L. Xu, S. Tang, Y. Cheng, K. Wang, J. Liang, C. Liu, Y.-C. Cao, F. Wei, L. Mai, Joule 2 (2018) 1991–2015.
[8] R. Khurana, J.L. Schaefer, L.A. Archer, G.W. Coates, J. Am. Chem. Soc. 136 (2014) 7395–7402.
[9] A. Manthiram, X. Yu, S. Wang, Nat. Rev. Mater. 2 (2017) 16103.
[10] H.K. Kitaura, A.S. Hayashi, T.K. Ohtomo, S.G. Hama, M.S. Tatsumisago, Mater. Chem. 21 (2011) 118–124.
[11] J.C. Bachman, S.K. Muy, A. Grimaud, H. Chang, N. Pour, S.F. Lux, O. Paschos, F. Maglia, S. K Lupart, P. Lamp, L. Giordano, Y.S. Horn, Chem. Rev. 116 (2016) 140–162.
[12] L.P. Yue, J. Ma, J.J. Zhang, J.W. Zhao, S.M. Dong, Z.H. Liu, G.L. Cui, L.Q. Chen, Energy Storage Mater. 5 (2016) 139–164.
[13] C. Sun, J. Liu, Y. Gong, D.P. Wilkinson, J. Zhang, Nano Energy 33 (2017) 363–386.
[14] W. Liu, S.W. Lee, D. Lin, F. Shi, S. Wang, A.D. Sendek, Y. Cui, Nat. Energy. 2 (2017) 17035.
[15] T.F. Miller III, Z.G. Wang, G.W. Coates, N.P. Balsara, Accounts Chem. Res. 50 (2017) 590–593.
[16] Z. Xue, D. He, X. Xie, J. Mater. Chem. 3 (2015) 19218–19235.
[17] B. Jinisha, K.M. Anilkumar, M. Manoj, V.S. Pradeep, S. Jayalekshmi, Electrochim. Acta 235 (2017) 210–222.
[18] J. Rolland, J. Brassinne, J.-P. Bourgeois, E. Poggi, A. Vlad, J.-F. Gohy, J. Mater. Chem. 2 (2014) 11839–11846.
[19] H. Zhang, C. Li, M. Piszcz, E. Coya, T. Rojo, L.M. Rodriguez-Martinez, M. Armand, Z. Zhou, Chem. Soc. Rev. 46 (2017) 797–815.
[20] H.J. Zhang, S. Kulkarni, S.L. Wunder, Phys. Chem. B 111 (2007) 3583–3590.
[21] J. Shim, D.G. Kim, H.J. Kim, J.H. Lee, J.C. Lee, ACS Appl. Mater. Interfaces 7 (2015) 7690–7701.
[22] E. Quartarone, P. Mustarelli, A. Magistris, Solid State Ionics 110 (1998) 1–14.
[23] L.Y. Yang, Z.J. Wang, Y.C. Feng, R. Tan, Y.X. Zuo, R.T. Gao, Y. Zhao, L. Han, Z. Q. Wang, F. Pan, Adv. Energy. Mater. 7 (2017) 1701437.
[24] W.D. Zhou, S.F. Wang, Y.T. Li, S. Xin, A. Manthiram, J.B. Goodenough, J. Am. Chem. Soc. 138 (2016), 9385-9338.
[25] F. Croce, G.B. Appetecchi, L. Persi, B. Scrosati, Nature 394 (1998) 456.
[26] S. Muench, A. Wild, C. Friebe, B. Häupler, T. Janoschka, U.S. Schubert, Chem. Rev. 116 (2016) 9438–9484.
[27] G. Li, S. Wang, Y. Zhang, M. Li, Z. Chen, J. Lu, Adv. Mater. 30 (2018) 1705590.
[28] W. Shin, J. Lu, X. Ji, Carbon Energy 1 (2019) 165–172.
[29] J. Xu, W. Zhang, H. Fan, F. Cheng, D. Su, G. Wang, Nano Energy 51 (2018) 73–82.
[30] F.Y. Fan, M.S. Pan, K.C. Lau, R.S. Assary, W.H. Woodford, L.A. Curtiss, W.C. Carter, Y.M. Chiang, J. Electrochem. Soc. 163 (2016) A3111–A3116.
[31] K. Takada, Acta Mater. 61 (2013) 759–770.
[32] A.G. Simmonds, J.J. Griebel, J.J. Park, K.R. Kim, W.J. Chung, V.P. Oleshko, J. Kim, E.T. Kim, R.S. Glass, C.L. Soles, Y.E. Sung, K.K. Char, J. Pyun, ACS Macro Lett. 3 (2014) 229–232.
[33] C.Z. Zhao, X.B. Cheng, R. Zhang, H.J. Peng, J.Q. Huang, R. Ran, Z.H. Huang, F. Wei, Q. Zhang, Energy Storage Mater. 3 (2016) 77–84.
[34] C. Barchasz, F. Molton, C. Duboc, J.-C. Leprêtre, S. Patoux, F. Alloin, Anal. Chem. 84 (2012) 3973–3980.
[35] R.D. Rauh, F.S. Shuker, J.M. Marston, S.B. Brummer, J. Inorg. Nucl. Chem. 39 (1977) 1761–1766.
[36] M.U.M. Patel, R. Demir-Cakan, M. Morcrette, J.-M. Tarascon, M. Gaberscek, R. Dominko, Chem. Sus. Chem. 6 (2013) 1177–1181.
[37] P. Dubois, J.P. Lelieur, G. Lepoutre, Inorg. Chem. 27 (1988) 73–80.
[38] K.H. Wujcik, J. Velasco-Velez, C.H. Wu, T. Pascal, A.A. Teran, M.A. Marcus, J. di Cabana, J.H. Guo, D. Prendergast, M. Salmeron, N.P. Balsara, J. Electrochem. Soc. 161 (2014) A1100–A1106.
[39] S. Zeng, L. Li, D. Zhao, D.K. Zhao, J. Liu, W.H. Niu, N. Wang, S.W. Chen, J. Phys. Chem. C 121 (2017) 2495–2503.
[40] H. Kim, J. Lee, H. Ahn, O. Kim, M.J. Park, Nat. Commun. 6 (2015) 7278.
[41] S. Chen, F. Dai, M.L. Gordin, Z. Yu, Y. Gao, J. Song, D. Wang, Angew. Chem. Int. Ed. 55 (2016) 4231–4235.
[42] M. Helen, M.A. Reddy, T. Diemant, U. Golla-Schindler, R.J. Behm, U. Kaiser, M. Fichtner, Sci. Rep. 5 (2015) 12146.
[43] R.X. He, T. Kyu, Macromolecules 49 (2016) 5637–5648.
[44] X. He, L. Wang, W. Pu, J. Ren, W. Wu, C. Jiang, C. Wan, J. Therm. Anal. Calorim. 94 (2008) 151–155.
[45] A. Petronico, T.P. Moneypenny, B.G. Nicolau, J.S. Moore, R.G. Nuzzo, A. A. Gewirth, J. Am. Chem. Soc. 140 (2018) 7504–7509.
[46] D. Saikia, A. Kumar, Electrochim. Acta 49 (2004) 2581–2589.
[47] H. Chen, H. Tu, C. Hu, Y. Liu, D. Dong, Y. Sun, Y. Dai, S. Wang, H. Qian, Z. Lin, L. Chen, J. Am. Chem. Soc. 140 (2018) 896–899.
[48] K.K. Kumar, M. Ravi, Y. Pavani, S. Bhavani, A.K. Sharma, V.V.R. Narasimha Rao, Phys. B Condens. Matter 406 (2011) 1706–1712.
[49] M.A. Ratner, D.F. Shriver, Chem. Rev. 88 (1988) 109–124.

[50] A.R. Polu, H.W. Rhee, Int. J. Hydrogen Energy 42 (2017) 7212–7219.
[51] R.C. Agrawal, G.P. Pandey, J. Phys. D Appl. Phys. 41 (2008) 223001.
[52] N. Jayaprakash, J. Shen, S.S. Moganty, A. Corona, L.A. Archer, Angew. Chem. Int. Ed. 50 (2011) 5904–5908.
[53] K. Park, J.H. Cho, J.H. Jang, B.C. Yu, T. Andreah, K.M. Miller, C.J. Ellison, J. B. Goodenough, Energy Environ. Sci. 8 (2015) 2389–2395.
[54] Y.R. Zhao, C. Wu, G. Peng, X.T. Chen, X.Y. Yao, Y. Bai, F. Wu, S.J. Chen, X.X. Xu, J. Power Sources 301 (2016) 47–53.
[55] S.H.S. Cheng, K.Q. He, Y. Liu, J.W. Zha, M. Kamruzzamana, R.L.W. Mad, Z. M. Dange, R.K.Y. Li, C.Y. Chung, Electrochim. Acta 253 (2017) 430–438.
[56] S.S. Zhang, K. Xu, T.R. Jow, Electrochim. Acta 49 (2004) 1057–1064.
[57] Y. Meesala, C.Y. Chen, A. Jena, Y.K. Liao, S.F. Hu, H. Chang, R.S. Liu, J. Phys. Chem. C 122 (2018) 14383–14389.
[58] C. Yu, S. Ganapathy, E.R.H. van Eck, H. Wang, S. Basak, Z.L. Li, M. Wagemaker, Nat. Commun. 8 (2017) 1086.

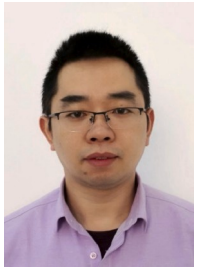

Chengguo Sun received his PhD degree in chemical engineering and technology at Nanjing University of Science and Technology, China in 2014. His is currently working as a postdoctoral researcher, cooperated with Prof. Feng Li as supervisor, at institute of Metal Research, Chinese Academy of Science, and also working as a full professor at University of Science and Techology Liaoning. His research interests are high-energy-density materials, electrocatalysts and all-solid-state lithium-ion batteries, aiming at preparation of the energetic cyclo-pentazolate salts and the high ionic conductivity of solid-state electrolytes.

Zhenxing Wang is currently a Ph.D student at the Institute of Metal Research, Chinese Academy of Sciences. He obtained his B.S. (2015) in Materials Science and Engineering from Jilin University in China. His research is focused on rational design of fluorinated interface for stable lithium metal anodes.

Dr. Lichang Yin is Professor of Shenyang National Laboratory for Materials Science, Institute of Metal Research, the Chinese Academy of Sciences. He received his Ph.D of Particle and Nuclear Physics in December 2002 from Jilin University of China. Then, he joined Prof. Huiming Cheng's group in 2003 as a postdoc. His current research activities focus on computational studies on energy conversion and energy storage materials.

Shengjun Xu received his BS degree in Chemistry from Fuzhou University in 2017, and currently he is a PhD candidate at Institute of Metal Research, Chinese Academy of Science and at University of Science and Technology of China. His research focuses on energy storage materials, solid polymer electrolytes and solid-state batteries.

Zahid Ali Ghazi received his PhD degree in Physical Chemistry from National Center for Nanoscience and Technology (NCNST), Beijing followed by a Postdoc in Prof. Feng Li's group at Institute of Metal Research (IMR), Chinese Academy of Sciences (CAS) China. His research interests focus on functional 2D nanomaterials for electrochemical energy storage devices, such as Li based batteries and supercapacitors.

Ying Shi is a research assistant working at the Advanced Carbon Division of the Institute of Metal Research, Chinese Academy of Sciences (IMR, CAS). She received her Bachelor's degree in 2006 and Master's degree in 2009 from the Department of Chemical Engineering, Dalian university of technology. Her research interests mainly focus on the development and application of carbon-based materials for energy storage.

Baigang An is a professor at University of Science and Techology Liaoning, China, received his Ph.D in the Applied Chemistry at Tianjin University in 2003. He had ever worked as a research fellow in Tohoku University Japan and a visiting scholar in Michigan University. In 2014, he was appointed as the head of excellent innovative teams of universities in Liaoning province, China. Since 2018 he is honored as a distinguished professor of Liaoning Province, China. He has published over 60 peer-reviewed papers. His current research interests include synthesis and application of nanomaterials in electrochemical storage and conversion of energy.

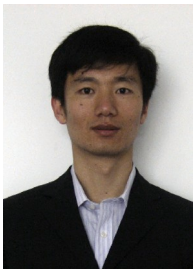

Zhenhua Sun received his B.S. and Ph.D. degrees in inorganic chemistry from Jilin University in 2001 and 2006, respectively. Then he was a Postdoctoral Research Fellow in the Chinese University of Hong Kong from 2007 to 2009. He is currently a professor at Institute of Metal Research, Chinese Academy of Science. His current research interests mainly focused on the synthesis and application of nano-carbon materials and carbon-based composite materials for electrochemical energy storage.

Dr. Hui-Ming Cheng is Professor and Director of both Advanced Carbon Research Division of Shenyang National Laboratory for Materials Science, Institute of Metal Research, Chinese Academy of Sciences, and the Low-Dimensional Material and Device Laboratory of the Tsinghua-Berkeley Shenzhen Institute, Tsinghua Univ. His research activities focus on carbon nanotubes, graphene, other two-dimensional materials, energy storage materials, photocatalytic semiconducting materials, and bulk carbon materials. He is recognized as a Highly Cited Researcher in both materials science and chemistry fields by Clarivate Analytics. He is now the founding Editor-in-Chief of Energy Storage Materials and the Associate Editor of Science China Materials.

Feng Li is a professor of Institute of Metal Research, Chinese Academy of Sciences (IMR, CAS). He received his Ph.D. in materials science at IMR, CAS in 2001 supervised by Prof. Hui-Ming Cheng. He mainly works on the novel carbon nanomaterials and energy materials. He has published more 300 papers on peer-reviewed journals such as Nat. Energy, Energ. Environ Sci., Adv. Mater., ACS Nano, Nano Energy, Energy Storage Mater. etc. with more 30000 citations and H-index about 80. He obtained the award of National Science Fund for Distinguished Young Scholars by National Foundation of Science, China and Highly Cited Researcher by Clarivate Analytics.